# NUMERICAL SIMULATION OF FBAR'S

**A. Reinhardt[†,‡,*], V. Laude[†], L. Robert[†], S. Ballandras[†], M. Solal[‡], W. Steichen[‡]**
[†]LPMO/CNRS associé à l'Université de Franche-Comté,
32 avenue de l'Observatoire, 25 044 Besançon Cedex, France
[‡]Temex Microsonics, 399 route des Crêtes, BP 232, 06 904 Sophia Antipolis Cedex, France

## Abstract

With the increase in operating frequencies of wireless communication standards, Thin Film Bulk Acoustic Resonators (FBAR's) are expected to become a key technology to provide miniature, high-performance and high-frequency filters. In this paper we briefly describe some models for simulating FBARs. We also discuss device optimization in terms of electromechanical coupling and characterization of fabricated devices. Finally, we show the interest of taking the exact geometry of devices into account.

## Introduction

With the increase in operating frequencies of new wireless communication standards, fabrication of Surface Acoustic Wave (SAW) devices becomes difficult. Dimensions of interdigitated transducers become very small. This increases the difficulty of the photolithography process. In order to produce SAW filters at frequencies above 3 GHz it is necessary to use expensive equipments, such as E-beam or X-Ray writers. This induces an increase in the unity cost of these components. Moreover the power handling of these devices also becomes problematic, as the acoustic power density flowing through the transducers becomes high. Thin Film Bulk Acoustic Resonators (FBAR's) tend to overcome these difficulties, and provide the possibility to design miniature, high-performance and high-frequency filters. Such resonators are basically made of a thin film of piezoelectric material vibrating in its thickness extensional mode [1]. With recent advances in thin film deposition, materials exhibit low mechanical losses, good electromechanical coupling factors, and high breakdown voltages for thicknesses in the order of 1 $\mu$m. These properties make resonators suitable for filter applications in the gigahertz range. Furthermore, one of the main advantages of FBARs is that their fabrication is compatible with standard IC processes. This enables the fabrication of resonators or filters along with other classical components on the same wafer. To our knowledge, oscillators or VCOs have already been fabricated and studied [1], [2].

Practical structures are reported in Figure 1. They are a little more complicated than the ideal electroded piezoelectric plate, as they require a substrate to support mechanically the resonator. This causes acoustic waves to propagate within the substrate and thus to make the composite structure vibrate at a much lower frequency. Though some devices, called Overmoded Resonators (OMR), use high harmonics of the fundamental thickness vibration of the substrate, when designing a resonator for filter applications, one usually want to get rid of the substrate's influence. A first solution is to locally etch the substrate so that only a thin support membrane remains under the piezoelectric layer and is made to vibrate. Other solutions require the isolation of the resonator from the substrate by either providing an air gap between them, fabricated by surface micromachining processes, or by depositing an acoustic Bragg mirror, made of alternative high and low impedance quarter wavelength layers, atop the substrate.

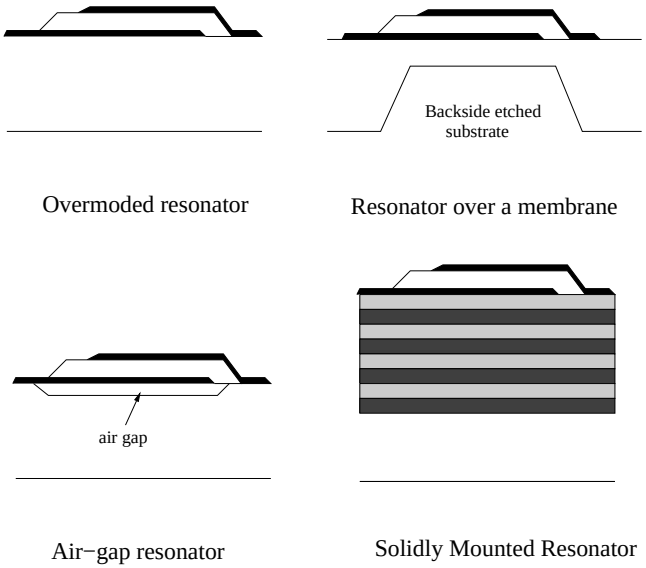


Figure 1: Practical resonator structures.

A few resonators need to be coupled together to produce a band pass filter. The most popular method is to use these resonators as impedance elements in ladder structures. Two types of resonators are fabricated to provide a resonance at two distinct frequencies. The changes in impedance with frequency lead to the filter response. The second way is to use mechanical rather than electrical coupling. Two resonators are stacked vertically, so that they lead to a set of coupled oscillators which exhibit two resonances, and thus a filter response. These filters are called Coupled Resonator Filters [3].

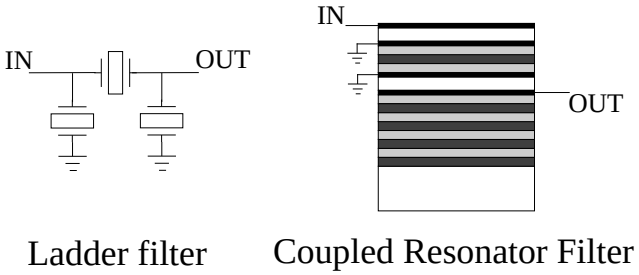


Figure 2: Practical filter structures.

To simulate such complex structures, efficient models need to be used. The simplest one is the Butterworth-Van Dyke lumped elements model describing the resonance of any acoustic resonator. Some improvements have been recently added to the particular case of FBAR structures [4], [5]. Its main interest is that it is widely used for fast device evaluation in process steps, but it cannot practically be used to predict the electrical response of resonators. The second model is Mason's which is the most widely used. It gives a rigorous calculation for one wave traveling in a multilayered medium, and as such is much more accurate than the lumped-elements representation. We prefer using a Fahmy-Adler representation of waves in multilayered materials [6]. Unlike Mason's model, it handles all acoustic modes that can propagate within a laminar layer. We have improved the original Fahmy and Adler's transfer matrix method so that is numerically more stable at high frequencies [7]. Though it is basically only one-dimensional and does not account for the shape of electrodes or the precise geometry of devices, it is useful in dimensioning layer thicknesses, and to provide a good idea of resonator performances, like resonant frequency, electromechanical coupling and quality factor. More complete models are based on the Finite Difference Time Domain (FDTD), on the Angular Spectrum method or on the Finite Element Method / Boundary Element Method (FEM/BEM) [8].

In a first part of this paper, we briefly describe some of the basic models used for simulating devices. We then focus on the characteristics of the different types of resonators and compare their capabilities. After that, we discuss the characterization of deposited materials using OMR's. Finally, we discuss more detailed simulations that can take geometric details into account.

**Simulation of acoustic waves in multilayers**

We make here a fast review of models available for the prediction of the behavior of waves in a multilayered medium. All these models provide finally the electrical response of devices implemented by a stack of material.

*Mason's model*

Mason's model is one of the most simple models that provide an accurate description of the propagation of a mode within a multilayered material. It deals with a pure mode, either of longitudinal or shear polarization, and the electric wave that propagates along with the mechanical wave. The characteristics of the propagation are given analytically as a function of the material properties. Also, by adding an imaginary part to the elastic and dielectric constants it becomes possible to take material losses into account.

The formulation of this model provides two equilibrium equations for one layer. These equations are solved using four boundary conditions:a mechanical and an electrical one on each side of the layer. For multilayered structures, assuming that mechanical displacements and electrical potential are continuous at the interface between two solids, it becomes possible to link the characteristics of the wave inside a layer to the characteristics in an other layer.

The main drawback of this model is that it can only deal with one mode and a given propagation direction. When changing the configuration, the characteristics of the new mode need to be recalculated. When exotic materials with specific crystalline orientations are to be considered, a few modes may exist simultaneously, and the model is no longer valid.

*Fahmy-Adler formulation*

The Fahmy-Adler formulation overcomes this problem. The vibration of a piezoelectric plate is described as the superposition of eight partial modes, two of which are purely electrostatic [6]. We have modified the original model to take into account perfectly conducting solids, by removing the two electrostatic partial modes [9]. We are also able to consider insulating fluids, like air for example, where the number of partial modes drops to four: two purely mechanical and of longitudinal polarization, and two purely electrostatic. These partial modes are obtained numerically in the case of solids by solving an eigenvalue problem, or analytically in the case of fluids. Thus, electromechanical fields in a layer are written as

$$\begin{aligned} \mathbf{h} &= (u_1, u_2, u_3, \Phi, T_{21}, T_{22}, T_{23}, D_2)^T \\ &= F\Delta(x_2)\mathbf{a}e^{j\omega(t-s_1x_1-s_3x_3)} \end{aligned} \quad (1)$$

where $u_i$ are the mechanical displacements components, $T_{2i}$ the components of the stress tensor that are continuous through the interface between two layers, $\Phi$ is the electric potential, and $D_2$ the electric normal displacement, $F$ is the matrix containing the polarization of all eigenmodes, $\Delta(x_2)$ is the diagonal matrix containing the propagation with depth terms and $\mathbf{a}$ the

vector containing the amplitudes of the partial modes. Axes conventions are shown in Fig. 3.

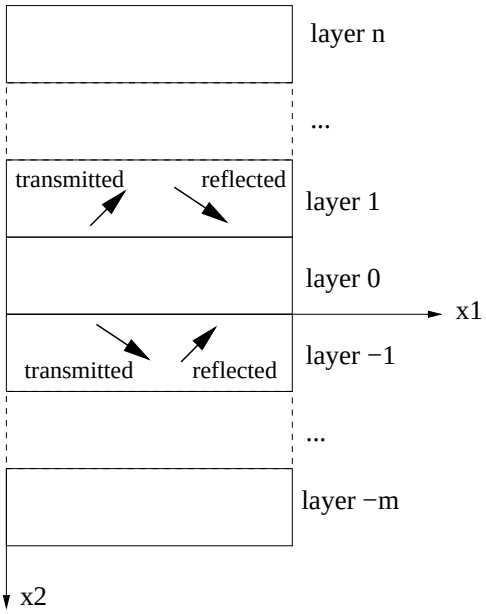


Figure 3: Axes definitions for a multilayered structure, and orientation of transmitted and reflected partial modes.

Within all the matrices in Eq. (1), partial modes are splitted into two groups, depending on their propagation direction, or the direction in which they are evanescent for inhomogeneous modes: these are called either transmitted from the excitation electrode, or reflected back to the excitation electrode, as depicted in Figure 3. The main purpose of the scattering matrix method is to compute reflexion matrices $R(x_2)$ that link amplitudes of partial reflected modes to amplitudes of partial transmitted modes:

$$\Delta^R(x_2)\mathbf{a}^R = R(x_2)\Delta^T(x_2)\mathbf{a}^T, \qquad (2)$$

where the subscripts $R$ and $T$ indicate the restriction of matrices to respectively the reflected or the transmitted partial modes. The algorithm starts at the interfaces limiting the electromechanical structure. In Figure 3, they correspond to the top of layer $n$ and the bottom of layer $-m$. On these surfaces, two types of boundary conditions are considered:either a semi-infinite medium, in which case no reflected modes are encountered in this layer, or a stress-free surface, which provides a relation between reflected and transmitted waves. In both cases, the reflection matrices at these surfaces are determined. A recursion scheme is then implemented, to transfer these matrices from one side of the layer to the other using the relation

$$R(x_2') = \Delta^R(x_2' - x_2)R(x_2)\Delta^T(x_2 - x_2'), \qquad (3)$$

where $x_2$ and $x_2'$ are coordinates in the same layer. A second step is to calculate the conversion of modes between two layers. This is achieved by writing the continuity of the displacements, the normal stresses, the potential, and the electric displacement. The two last components may be assumed zero if a conducting layer other than the excitation electrode is encountered. Then, these steps are repeated until boundary conditions applied to the multilayer have been transfered to the boundary of the excitation electrode layer. It is then written that the electric potential is forced to a normalization value of 1 in the neighboring insulating layers, and that mechanical components stay continuous through the limits of the electrode layer. This provides a relation giving the amplitudes of all partial modes in the layers number -1, 0 or 1 proportional to the input voltage. Then it is possible to calculate the currents in the electrode, given by the discontinuity of the electric displacements between insulating media and the metal, and the applied potential, which provides the electric admittance of the device. On the other hand, we have already determined the mode conversion relation at each interface, so that it is possible to determine the amplitudes of partial modes in every layer. This allows us to study standing wave patterns within any multilayer. This method will be described in much more details in a forthcoming paper [9].

In the following of this paper, resonator performances are described in terms of quality factor $Q$ of the resonance, and of electromechanical coupling, that is calculated using the determination of resonance $f_R$ and antiresonance $f_A$ frequency, as given by the standard formula [10]

$$k^2 = \frac{\pi^2}{4}\frac{f_A - f_R}{f_R}. \qquad (4)$$

**Simulation of resonators**

The basis of the simulation has been described in the previous section. We are now looking at the simulation of resonator structures.

*Overmoded Resonators*

In the OMR configuration, a bulk wave resonator is put directly atop a thick substrate. So, vibration occurs not only in the thin film layer, but also in the substrate. This leads to a very low fundamental resonant frequency, in the order of around 10 MHz for a nearly 400 $\mu$m thick silicon wafer. As most of the acoustic path is located within the substrate, properties of the resonator are mostly given by the substrate's properties. This is why such resonators are usually made with high quality materials. To reach the gigahertz range, it is also necessary to use high order harmonics. But in that case, the resonance peaks are very close to each other, and are difficult to discriminate. An example of the simulated

response of such a device is shown in Figure 4:the quality factor is very high, as the substrate is monocristalline silicon, but the electromechanical coupling is very low, as high order harmonics are examined.

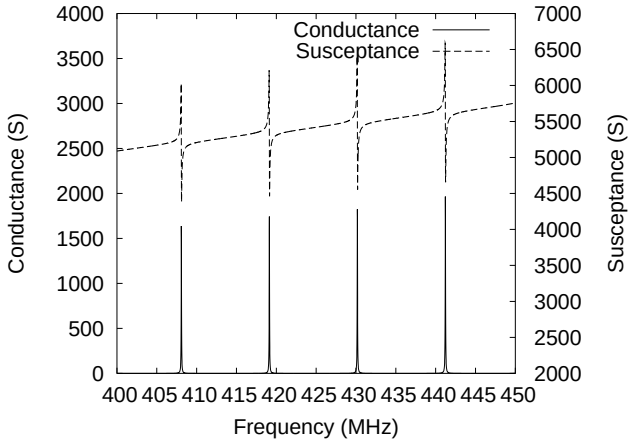


Figure 4: Response of an overmoded resonator.

*Air-gap Resonators*

The interface between the electrode material and air provides the isolation needed for the resonator to operate like the ideal electroded plate. Air has such a low acoustic impedance that the acoustic power transmitted through the air-gap is neglectible and cannot really make the substrate vibrate. Despite this behavior, it is the most complicated structure to fabricate. The first main technological challenge is the deposition of a sacrificial layer that needs to be etched when releasing the piezoelectric membrane. There may remain some material underneath the membrane, what deteriorates the response of the resonator. The second difficulty is to produce a low-stress membrane so that it remains quite flat and does not break when it is released. Finally, such a membrane is very sensitive to chocks, unlike more monolithic structures, like the OMR or the SMR.

As resonators operate at a very high frequency, the thickness of electrodes does no more remain neglectible. Their effect has then been investigated. They mainly cause a resonance shift due to the mass-loading, or the extension of the resonant cavity size, but this effect is not linear, as shown in Fig. 5. It also depends on the mass of the electrode. A second effect is that the electromechanical coupling coefficient has an optimum. This is due to phase matching between the longitudinal mode in the resonator and the electrostatic one. The optimum gets higher for a metal with a high acoustic impedance, as reflexions at the interface between metal and piezoelectric provide some energy trapping within the piezoelectric.

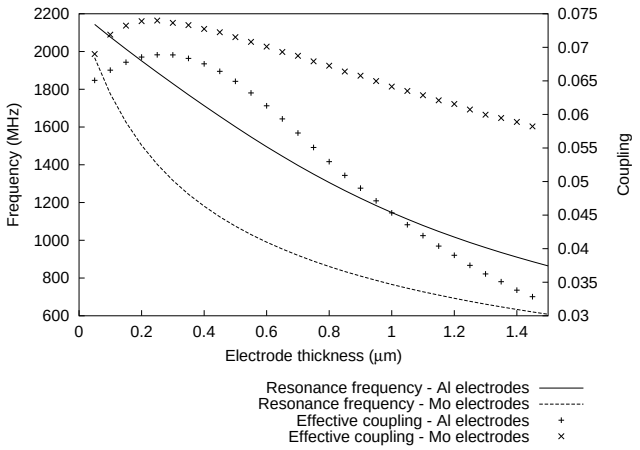


Figure 5: Resonant frequency shift and coupling coefficient enhancement vs. electrode thickness. These curves correspond to a 2.5 $\mu$m thick AlN membrane, with either aluminum or molybdenum electrodes.

*Solidly Mounted Resonators*

As stated above, a SMR is made of a resonator fabricated atop a Bragg mirror, composed of quarter-wavelength layers of alternatively high and low impedance materials. The effect of these layers is to lower the acoustic impedance of the substrate so that nearly total reflection of the waves occurs at the bottom of the resonator. This ensures that the acoustic power remains localized within the piezoelectric layer and thus that the resonator exhibits a good electromechanical coefficient. Examples of reflection coefficient of Bragg mirrors are shown in Figure 6 for two materials combinations. These coefficients have been extracted by taking the component of the reflexion matrix which corresponds to the reflexion of the longitudinal wave in the metal at the bottom of the bottom electrode of the resonator. The number of layers pairs needed and the width of the frequency band in which the mirror provides a good reflection coefficient are functions of the impedance ratio of the two materials used. But whatever their nature, the bandwidth of the mirror is wide enough to reject modes linked to the reflection on the back side of the substrate.

Once the mirror is designed, the resonator itself must be optimized. This is performed by adjusting the thicknesses of the electrodes, which is the last parameter to adjust. These exhibit the same kind of effects as the air-gap resonator. But here, in Fig. 7 the frequency has been kept constant by adjusting the thickness of the piezoelectric layer.

**Device characterization**

In order to accurately simulate FBAR devices we need to use well-characterized material constants. In this view we have fabricated devices and characterized

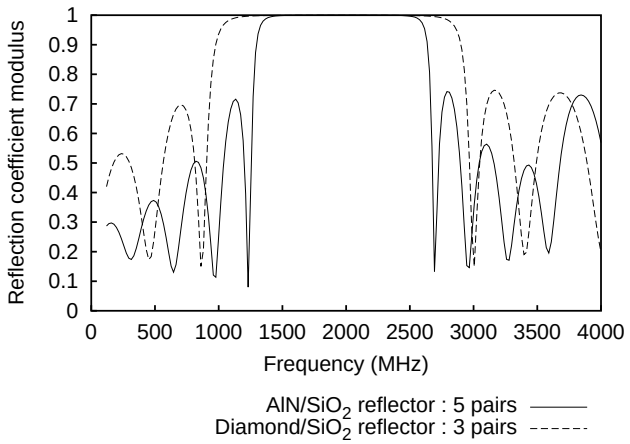


Figure 6: Reflection coefficients of two Bragg mirrors:AlN/$SiO_2$ (impedance ratio 2.17) and Diamond/$SiO_2$ (impedance ratio 3.59).

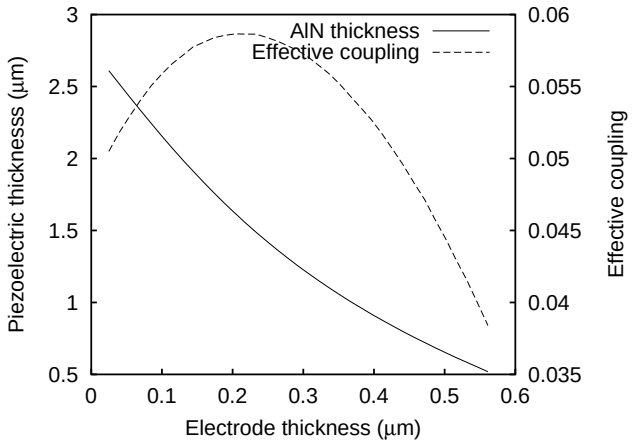


Figure 7: Effect of electrodes thickness:piezoelectric thickness needed to ensure a constant resonance frequency and electromechanical coupling.

them. They were made in the OMR configuration:a 2 $\mu$m thick AlN film DC-sputtered with 200 nm thick aluminum electrodes over a 380 $\mu$m silicon wafer. Electrical measurements were fitted by varying AlN material constants, while fixing silicon and aluminum properties, which are well-known since they have already been used for many applications. In the fit progress, coupling is directly related to the $e_{33}$ parameter, the static capacitance to $\epsilon_{33}$, the quality factor to mechanical losses and the floor of the admittance curve is due to the dielectric loss tangent of the material. A rigorous analysis would also consider ohmic losses in the electrodes, but we rather include them in the loss tangent. The only constant that cannot reasonably be fitted is $c_{33}$ because the tolerances upon the thicknesses of all layers are sufficiently large to have them account for the exact location of the resonance frequency. Such a fit is shown in Figure 8.

To overcome the problem of determining the elastic

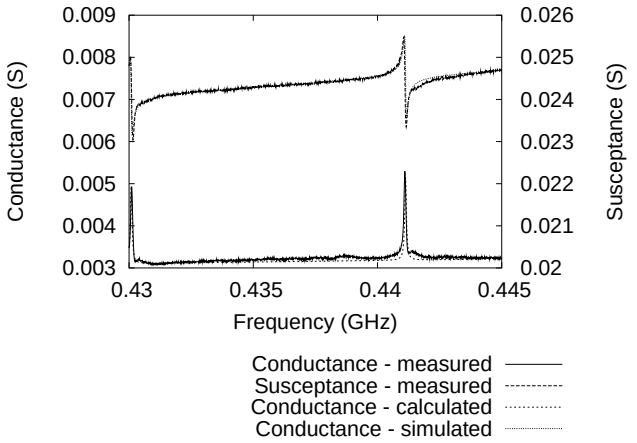


Figure 8: Device measurements versus fitted response.

constant of the piezoelectric layer, we etch the backside to reduce the thickness of the substrate. This way, the dependence of the resonance upon the substrate's properties is lowered, and by comparing different measures of the same device for multiple substrate thicknesses it is possible to determine more accurately the piezoelectric's properties. Fitted values are reported in Table 1. These values are not as high as those found in the literature, but the deposition process is currently being optimized. Losses are also overestimated as we take a very low mechanical loss tangent ($10^{-4}$) for silicon, but further measurements should help to solve this point.

We have also investigated the temperature dependence of aluminum nitride. The wafers were heated by a thermal chuck during probing and the frequency shift of the resonators was measured. In Fig. 9, we report the experimental relative frequency variations of various harmonics for two substrate thicknesses. It seems that all harmonics have almost the same temperature sensibility:-34 ppm/K. We have used the Campbell and Jones approach, which considers that the temperature effects are caused by the dependency of elastic constants with temperature, and by the thermal expansion of the layers. This has been added to our scattering matrix model, and gives almost the same temperature sensitivity for simulated devices, as can be seen in Fig. 9. This shows that temperature coefficients found in literature apply well to our experiments. Another fact is that the thickness of the substrate does not seem to change the temperature behavior. An early explanation is that the reduction of the substrate's thickness is not sufficient to induce a significant temperature dependence change, compared to the dispersion of the results. Further investigations are needed to determine more accurately the influence of the AlN layer.

Table 1: Fitted material constants

| Aluminum nitride parameters | Fitted values | Values from literature [12] |
|---|---|---|
| $c_{33}$ (cannot be determined accurately) | 395 GPa | 395 GPa |
| mechanical loss tangent | 0.1 | $5.10^{-4}$ |
| $e_{33}$ | 1.5 C/m$^2$ | 1.55 C/m$^2$ |
| $\epsilon_{33}$ | 9.5 $10^{-11}$ F/m | 9.5 $10^{-11}$ F/m |
| dielectric loss tangent | 0.12 | 0 |

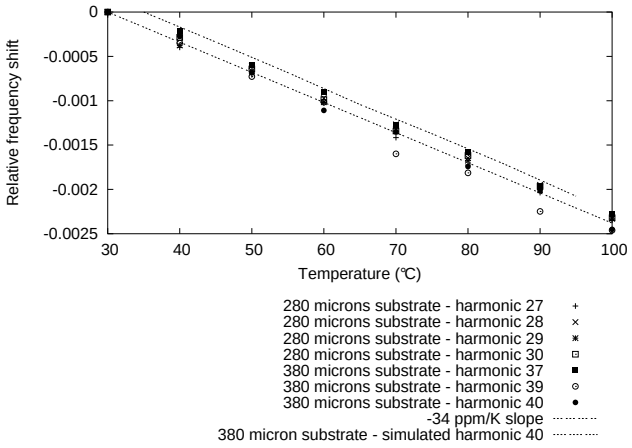


Figure 9: Relative frequency shift with temperature for various harmonics on various substrate thicknesses. All modes are located in the same frequency range.

**Simulation of geometrical effects**

Now that we have shown how to use simple models to predict the electrical response of FBAR resonators, and that we have shown how these models are adjusted to the material properties, we discuss in the following of this paper the full simulation of effects caused by the exact geometry of devices.

*Angular Spectrum of Waves*

The first model we expose is the Angular Spectrum of Waves. The principle is to consider that the response of a device is the superposition of the contributions of all the waves propagating with every direction into the multilayer. Thus, the method is well suited to consider the width of the upper electrodes of a resonator. Calculations are performed in two steps: first, the spectral charge distribution under the electrodes is determined. This is performed after expanding electrical charge and potential at the surface on a Tchebyshev polynomials basis. Then, using the spectral Green's function at the surface of the multilayer, which is calculated using the scattering matrix method described earlier, the relation between charge and potential is determined. Details of the calculations are very similar to the ones of a FEM/BEM method developed to analyze SAW gratings on a semi-infinite substrate [13], though in our case we do not really know the singularities of the electrostatic Green's function and have to perform a numerical integration over the surface wave vectors. If only the electric response is needed, calculations can be stopped here. A second step is to calculate the acoustic field distribution in the multilayer. This is obtained by calculating for each wave vector along the surface the generated fields within the structure. The global fields are given as the superposition of all these generated fields, weighted by the spectral charge distribution.

Some early results have been obtained to validate the model. We have considered a simple resonator, and compared the response obtained with the Angular Spectrum model to the one obtained by the classical monodimensional one. This is shown in Fig. 10. Resonance and antiresonance frequencies match very well. It seems also that the quality factor becomes much lower when shrinking the size of electrodes. But these are still early results and should be considered with care. Especially, they should be correlated with those obtained from a classical Finite Element Method (FEM) software.

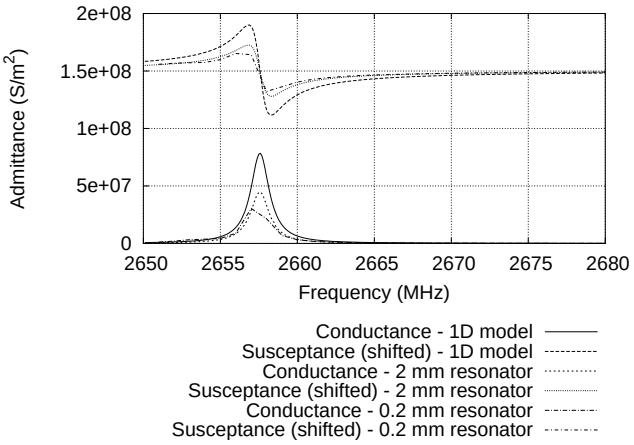


Figure 10: Validation of the Angular Spectrum of Waves.

*Finite Element Analysis*

For more precise details to be taken into account, FEM/BEM methods need to be used. In practice, we use a periodic FEA/BEM approach, which is much more detailed in two other papers of this congress [8], [14]. We do not recall the principle here, but the sim-

ulation method consists in meshing the inhomogeneous part, that is handled by the FEM part of the model. Radiation in the surrounding environment is calculated using spectral Green's functions, which is determined by the scattering matrix algorithm described earlier. Here we do not consider periodicity and set $\gamma$ defined in [8], [14] to zero.

In a first step we simulate an air-gap resonator using the mesh shown in Fig. 11: an aluminum nitride membrane is build as a bridge over the substrate. The admittance curve is shown in Fig. 12. It can be seen that it exhibits some irregularities just before the resonance frequency, that could be accpunted for by the flexion of the pads supporting the membrane. These effects could not be seen when using a one dimensional model. We


Figure 11: Mesh of an air-gap resonator.

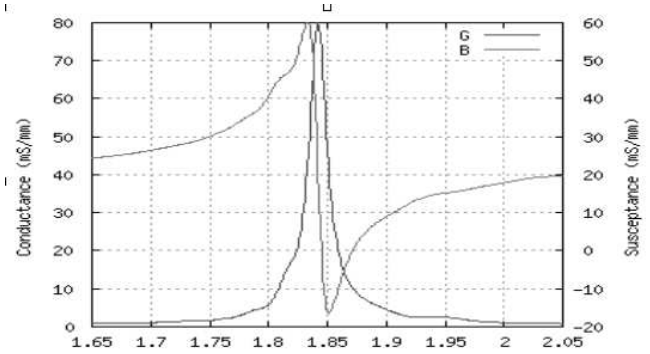


Figure 12: Electrical response of an air-gap resonator.

then report the simulation of a Solidly Mounted Resonator, whose mesh is shown in Fig. 13. For this device, the geometry effects are even more visible in Fig. 14 than for the air-gap resonator.

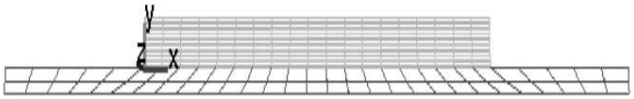


Figure 13: Mesh of a SMR.

## Conclusion

We have presented an overview of some of the different approaches available for the simulation and the design of thin film BAW resonators, with emphasize on the Fahmy-Adler and the scattering matrix model which

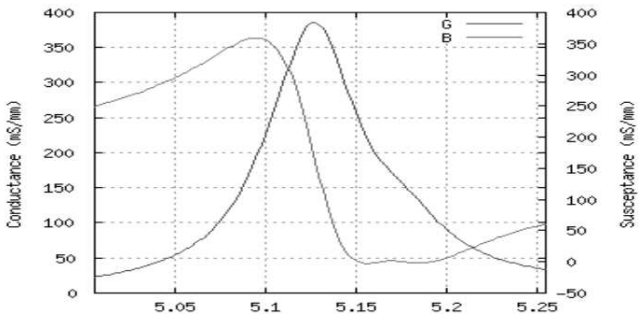


Figure 14: Electric response of a SMR.

is a semi-analytical model well suited for simple simulations of FBARs, but can also be involved in more complex models. We have characterized the material properties of AlN deposited at LPMO, though the optimization of the process remains under work and though more samples need to be measured to improve the validity of our characterization. We have also shown that geometry effects affect the electric response of resonators, so that it is necessary to use more complex models. In this paper we have given the example of a periodic FEM/BEM analysis under synchronous excitation, but we are currently working on a semi-analytical model, based on the Angular Spectrum of Waves.

## Acknowledgments

The authors want to thank Pascal Blind, from the Centre de Transfert des Microtechniques, who has performed the etching of the substrates.

## References

[1] K. M. Lakin, G. R. Kline, R. S. Ketcham, A. R. Landin, W. A. Burkland, K. T. McCarron, S. D. Braymen, and S. G. Burns, "Thin film resonator technology" in 41st Annual Frequency Control Symposium, 1987, pp. 371-381.

[2] Park, Y.S. and Pinkett, S. and Kenney, J.S. and Hund, W.D., "A 2.4 GHz VCO with an Integrated Acoustic Solidly Mounted Resonator", in Proceedings of 2001 Ultrasonics Symposium, Atlanta, USA, pp. 839-842.

[3] K.M. Lakin, "Coupled Resonator Filters", in Proceedings of 2002 IEEE Ultrasonics Symposium, Munich, Germany, pp. 879-886.

[4] Larson III, J.D. and Bradley, P.D. and Wartenberg, S. and Ruby, R.C., "Modified Butterworth-Van Dyke Circuit for FBAR Resonators and Automated Measurement System", in Proceedings of 2000 IEEE Ultrasonics Symposium, pp. 863-868.

[5] M.C. Chao, S.Y. Bao, Z.N. Huang, Z. Wang, and C.S. Lam, , "Modified BVD-Equivalent Circuit of FBAR by taking Electrodes into Account", in Proceedings of 2002 IEEE Ultrasonics Symposium, Munich, Germany, pp. 848-851.

[6] E. L. Adler, "Matrix Methods Applied to Acoustic Waves in Multilayers" IEEE Transactions on Ultrasonics and Frequency Control, vol. 37, pp. 485-490.

[7] T. Pastureaud, V. Laude and S. Ballandras, "Stable scattering-matrix method for surface acoustic waves in piezoelectric multilayers" Applied Physics Letters, vol. 80, pp. 2544-2546.

[8] S. Ballandras, M. Wilm, V. Laude, W. Daniau, F. Lanteri, J.F. Gelly, O. Burat, R. Lardat, T. Pastureaud, "2D and 3D finite element/boundary element computations of periodic piezoelectric transducers radiating in stratified media", presented at 2003 World Congress of Ultrasound, Paris, France.

[9] A. Reinhardt, T. Pastureaud, S. Ballandras and V. Laude, "Scattering matrix method for modeling acoustic waves in piezoelectrics, fluid and metallic multilayers", submitted to the Journal of Applied Physics.

[10] "ANSI/IEEE Std. 176-1987, IEEE Standard on Piezoelectricity"

[11] A. Reinhardt, V. Laude, T. Pastureaud and S. Ballandras "Numerical simulation and comparison of membrane and solidly mounted FBAR's" in Proceedings of 2002 IEEE Ultrasonics Symposium, Munich, Germany, pp. 480-483.

[12] G. Carlotti, F. S. Hickernell, H. M. Liaw, L. Palmieri, G. Socino and E. Verona "The Elastic Constants of Sputtered Aluminum Nitride Films" in Proceedings of 1995 Ultrasonics Symposium, pp. 353-356.

[13] P. Ventura, J.M. Hodé, B. Lopes, "Rigorous Analysis of Finite SAW Devices with Arbitrary Electrode Geometries", in Proceedings of 1995 IEEE Ultrasonics Symposium, pp. 257-262.

[14] S. Ballandras, V. Laude, T. Pastureaud, M. Wilm, W. Daniau, A. Reinhardt, W. Steichen, R. Lardat, "A FEA/BEM Approach to Simulate Complex Electrode Structures Devoted to Guided Elastic Wave Periodic Transducers", presented at 2003 World Congress of Ultrasound, Paris, France.